

DIRECT FABRY-PÉROT EFFECT REMOVAL

WITHAWAT WITHAYACHUMNANKUL

*Department of Information Engineering, Faculty of Engineering,
King Mongkut's Institute of Technology Ladkrabang, Bangkok 10520, Thailand
Centre for Biomedical Engineering and Department of Electrical & Electronic Engineering,
The University of Adelaide, SA 5005, Australia
withawat@eleceng.adelaide.edu.au*

BRADLEY FERGUSON

*Centre for Biomedical Engineering and Department of Electrical & Electronic Engineering,
The University of Adelaide, SA 5005, Australia
Tenix Systems Pty Ltd, 2nd Avenue, Mawson Lakes, SA 5095, Australia
brad.ferguson@tenix.com*

TAMATH RAINSFORD, SAMUEL MICKAN and DEREK ABBOTT

*Centre for Biomedical Engineering and Department of Electrical & Electronic Engineering,
The University of Adelaide, SA 5005, Australia
tamath@eleceng.adelaide.edu.au, spmickan@eleceng.adelaide.edu.au and
dabbott@eleceng.adelaide.edu.au*

Received 30 June 2005

Accepted 22 March 2006

Communicated by Stuart Tessmer

This study indicates that the removal of reflections from T-ray signals can be carried out in the frequency domain without prior knowledge of material parameters or sample thickness. By fitting polynomials to the logarithm and the argument of the sample's transfer function, the Fabry-Pérot reflection term is canceled out, leading to disappearance of the reflections in spatial domain. The method successfully removes the reflections for optically thick samples under the condition of noise or amplitude fluctuations. The application to optically thin samples is possible when the samples are subjected to broadband terahertz measurements. The Fabry-Pérot free signal, when used as input to the parameter estimation method, results in correct material parameters with low variance.

Keywords: Fabry-Pérot removal; reflection; T-rays; terahertz time-domain spectroscopy; gradient-based parameter estimation; noise in photonic measurement systems.

1. Introduction

T-rays, spanning the range from 0.1 to 10 THz in electromagnetic spectrum, have been attracting researchers in many fields. T-ray systems, in the past, hardly

delivered utilizable signals due to the lack of efficient sources and detectors. Furthermore, there was the difficulty of background black-body radiation in the terahertz range. Since then, T-ray systems have been continually developed to the point where time-gated detection techniques in free space achieved SNRs of the order of 170 dB and beyond [1]. Owing to a number of useful properties, T-rays have the potential for a broad range of applications including medical diagnosis, industrial quality control, airport security, and so on [2, 3]. One of the most widely-used applications is materials characterization using terahertz time-domain spectroscopy (THz-TDS) [4].

Based on terahertz time-domain spectroscopy (THz-TDS), material parameter extraction [5–9] and material classification [10–13] basically need two T-ray signals, a reference and a sample-probing signal, in order to compute a system-independent frequency response of a sample under test. The sample-probing signal typically contains unwanted Fabry-Pérot reflections. These are unwanted as they are a source of measurement error. For a material with low refractive index, the amplitude of the reflections is so small that they are negligible. However, when probing a material with high refractive index, the reflections arise and a method to remove them from the signal becomes necessary.

This article is organized as follows. Prior work proposing methods to remove the Fabry-Pérot effect is briefly reviewed in Sec. 2. In Sec. 3 a simple transfer function is developed on the basis of a T-ray propagation model in a planar homogeneous material. This leads to the removal of the Fabry-Pérot term in the model. Section 4 demonstrates the removal of Fabry-Pérot term in two simulated environments, one for an optically thick sample and the other for an optically thin sample, both of which are subjected to strong noise. In Sec. 5 our method is employed to remove reflections from a T-ray signal, which is used to probe a test sample composed of silicon.

2. Prior Work

So far there is no direct and efficient method to discern the reflections caused by the Fabry-Pérot effect from a detected T-ray signal. One of the existing methods is to window the signal in the spatial domain [5]. However, it requires prior knowledge of sample thickness, refractive indices, and pulse width to precisely locate the position of reflections. Moreover, this method fails to isolate the reflections from the primary pulse for an optically-thin sample, since the reflections spatially overlap the primary pulse. Besides, it cannot distinguish the reflections when the primary pulse possesses long fluctuations. Other methods deal with the reflections along with the parameter extraction process [5–7], where efficiency is degraded by iterative techniques.

The method proposed in this paper locates and discriminates the reflections from the required signal directly. By approximating the transfer function of the sample with a simpler model, the reflections can be estimated and subtracted from the probing signal, leaving only the primary pulse. Since the method is performed in frequency domain, it can correctly remove the reflections regardless of the sample thickness or material parameters. Moreover, no iterative procedure is required by the process, thus leading to efficient real-time application.

3. Theory

3.1. Transfer function for T-rays propagating in homogeneous material

Given a T-ray signal transmitted through the sample at normal incidence, $E_{\text{sample}}(t)$, and a reference signal traveling an identical path without the presence of the sample, $E_{\text{ref}}(t)$, a measured transfer function, obtained by deconvolving the probe signal spectrum with respect to the reference spectrum, is described by [5, 7]:

$$H(\omega) = \frac{E_{\text{sample}}(\omega)}{E_{\text{ref}}(\omega)} = \frac{4\tilde{n}_{\text{sample}}\tilde{n}_{\text{air}}}{(\tilde{n}_{\text{sample}} + \tilde{n}_{\text{air}})^2} \cdot \exp \left[-i(\tilde{n}_{\text{sample}} - \tilde{n}_{\text{air}}) \frac{\omega L}{c} \right] \cdot \text{FP}(\omega), \quad (1)$$

where L is the sample thickness, and $\tilde{n}_{\text{sample}}$ and \tilde{n}_{air} are the complex refractive indices of sample and air, respectively. The complex refractive index contains two components: a real refractive index n and an absorption index κ , where $\tilde{n} = n - i\kappa$. Note that both n and κ are frequency-dependent, but for simplicity we drop the frequency dependent notation, unless otherwise stated. In Eq. (1), $\text{FP}(\omega)$ represents the Fabry-Pérot effect or the interference in the received signal from reflections within the material,

$$\text{FP}(\omega) = \frac{1}{1 - \left(\frac{\tilde{n}_{\text{sample}} - \tilde{n}_{\text{air}}}{\tilde{n}_{\text{sample}} + \tilde{n}_{\text{air}}} \right)^2 \cdot \exp \left[-2i\tilde{n}_{\text{sample}} \frac{\omega L}{c} \right]}. \quad (2)$$

3.2. Simple model for magnitude of the transfer function

We propose to replace the transfer function by a simpler equation. Real and imaginary parts of the function are not continuous, so estimation by any other simpler model is usually considered to be not feasible. On the other hand, the absolute magnitude and argument of the transfer function are appropriate since they are continuous variables.

The logarithm of the transfer function is given by

$$\ln |H(\omega)| = \ln \left| \frac{4\tilde{n}_{\text{sample}}\tilde{n}_{\text{air}}}{(\tilde{n}_{\text{sample}} + \tilde{n}_{\text{air}})^2} \right| - \kappa_{\text{sample}} \frac{\omega L}{c} + \ln |\text{FP}(\omega)|. \quad (3)$$

The first term on the RHS is almost constant over the range of frequency, while the second term for a given absorption index depends on the frequency. Hence these two terms can be combined and represented by a power series. Equation (3) is then rewritten in a simpler form as

$$\ln |H(\omega)| \equiv a_0 + a_1\omega + \dots + a_k\omega^k + \ln |\text{FP}(\omega)|. \quad (4)$$

This model can be used to describe data from the measured transfer function in place of the general model in Eq. (3). A residue or a difference between this model and the real data is given by sum of square of offsets along a frequency range,

$$R^2 \equiv \sum_i \left\{ \Gamma_i - (a_0 + a_1\omega_i + \dots + a_k\omega_i^k + \ln |\text{FP}(\omega_i)|) \right\}^2, \quad (5)$$

where $\Gamma_i = \ln |H_{\text{meas}}(\omega_i)|$. The a_k coefficients are obtained by the least squares fitting method. We take a partial derivative of the residue w.r.t. each coefficient

and equate it to zero, or

$$\begin{aligned} \frac{\partial(R^2)}{\partial a_0} &= -2 \sum_i \{ \Gamma_i - (a_0 + a_1 \omega_i + \dots + a_k \omega_i^k + \ln |\text{FP}(\omega_i)|) \} = 0 \\ \frac{\partial(R^2)}{\partial a_1} &= -2 \sum_i \{ \Gamma_i - (a_0 + a_1 \omega_i + \dots + a_k \omega_i^k + \ln |\text{FP}(\omega_i)|) \} \omega_i = 0 \\ \frac{\partial(R^2)}{\partial a_k} &= -2 \sum_i \{ \Gamma_i - (a_0 + a_1 \omega_i + \dots + a_k \omega_i^k + \ln |\text{FP}(\omega_i)|) \} \omega_i^k = 0. \end{aligned} \tag{6}$$

This leads to

$$\begin{aligned} a_0 N + a_1 \sum_i \omega_i + \dots + a_k \sum_i \omega_i^k + \sum_i \ln |\text{FP}(\omega_i)| &= \sum_i \Gamma_i \\ a_0 \sum_i \omega_i + a_1 \sum_i \omega_i^2 + \dots + a_k \sum_i \omega_i^{k+1} + \sum_i \omega_i \ln |\text{FP}(\omega_i)| &= \sum_i \omega_i \Gamma_i \\ a_0 \sum_i \omega_i^k + a_1 \sum_i \omega_i^{k+1} + \dots + a_k \sum_i \omega_i^{2k} + \sum_i \omega_i^k \ln |\text{FP}(\omega_i)| &= \sum_i \omega_i^k \Gamma_i. \end{aligned} \tag{7}$$

We rewrite the Fabry-Pérot term, in Eq. (2), in a simplified form as follows

$$\text{FP}(\omega) \equiv \frac{1}{1 - \alpha \cdot \exp(-i\theta)}, \tag{8}$$

where

$$\theta = 2n_{\text{sample}} \frac{\omega L}{c}, \tag{9}$$

and

$$\alpha = \left(\frac{n_{\text{sample}} - n_{\text{air}}}{n_{\text{sample}} + n_{\text{air}}} \right)^2 \exp \left(-2\kappa_{\text{sample}} \frac{\omega L}{c} \right). \tag{10}$$

For the sake of simplicity, the n_{sample} and κ_{sample} are assumed to be constant over the frequency range of interest, and the value of n_{sample} is much larger than that of κ_{sample} . Hence, the summation of the Fabry-Pérot terms in Eq. (7) is

$$\begin{aligned} \sum_i \omega_i^k \ln |\text{FP}(\omega_i)| &= \sum_i \{ \omega_i^k \ln(1) - \omega_i^k \ln |1 - \alpha_i \exp(-i\theta_i)| \} \\ &= - \sum_i \omega_i^k \ln |1 - \alpha_i \cos \theta_i + i\alpha_i \sin \theta_i| \\ &= -\frac{1}{2} \sum_i \omega_i^k \ln (1 - 2\alpha_i \cos \theta_i + \alpha_i^2 \cos^2 \theta_i + \alpha_i^2 \sin^2 \theta_i) \\ &= -\frac{1}{2} \sum_i \omega_i^k \ln (1 - 2\alpha_i \cos \theta_i + \alpha_i^2) \\ &\approx \frac{1}{2} \sum_i \omega_i^k (2\alpha_i \cos \theta_i - \alpha_i^2) \\ &= \sum_i \omega_i^k \alpha_i \cos \theta_i - \frac{1}{2} \sum_i \alpha_i^2. \end{aligned} \tag{11}$$

Compared to $\sum_i \omega_i^k$ of Eq. (7), the $\sum_i \omega_i^k \ln |\text{FP}(\omega_i)|$ gives a much smaller value caused by a rapid decay of the exponent and an averaging summation of the cosine, according to Eq. (11). Therefore, we can approximate all Fabry-Pérot terms of Eq. (7) to zero. This relation implies that if the measured data, $\ln |H_{\text{meas}}(\omega)|$, is fitted by

$$f_1(\omega) = a_0 + a_1\omega + \dots + a_k\omega^k, \tag{12}$$

the Fabry-Pérot terms are small.

3.3. Simple model for argument of the transfer function

The negligible contribution of the Fabry-Pérot terms also occurs when an argument of the transfer function is fitted by a power series. Given the argument of the transfer function

$$\arg[H(\omega)] = \arg \left[\frac{4\tilde{n}_{\text{sample}}\tilde{n}_{\text{air}}}{(\tilde{n}_{\text{sample}} + \tilde{n}_{\text{air}})^2} \right] - (n_{\text{sample}} - n_{\text{air}}) \frac{\omega L}{c} + \arg[\text{FP}(\omega)], \tag{13}$$

we can simplify it to

$$\arg[H(\omega)] \equiv b_0 + b_1\omega + \dots + b_k\omega^k + \arg[\text{FP}(\omega)], \tag{14}$$

because the first term on the RHS of Eq. (13) is almost constant while the succeeding term depends on the frequency. The residue between our model and the measured data is given by

$$R^2 \equiv \sum_i \{ \Lambda_i - (b_0 + b_1\omega_i + \dots + b_k\omega_i^k + \arg[\text{FP}(\omega_i)]) \}^2, \tag{15}$$

where $\Lambda_i = \arg[H_{\text{meas}}(\omega_i)]$. Taking a partial derivative of the residue w.r.t. each coefficient and equating it to zero yields

$$\begin{aligned} \frac{\partial(R^2)}{\partial b_0} &= -2 \sum_i \{ \Lambda_i - (b_0 + b_1\omega_i + \dots + b_k\omega_i^k + \arg[\text{FP}(\omega_i)]) \} = 0 \\ \frac{\partial(R^2)}{\partial b_1} &= -2 \sum_i \{ \Lambda_i - (b_0 + b_1\omega_i + \dots + b_k\omega_i^k + \arg[\text{FP}(\omega_i)]) \} \omega_i = 0 \\ \frac{\partial(R^2)}{\partial b_k} &= -2 \sum_i \{ \Lambda_i - (b_0 + b_1\omega_i + \dots + b_k\omega_i^k + \arg[\text{FP}(\omega_i)]) \} \omega_i^k = 0, \end{aligned} \tag{16}$$

or

$$\begin{aligned} b_0 N + b_1 \sum_i \omega_i + \dots + b_k \sum_i \omega_i^k + \sum_i \arg[\text{FP}(\omega_i)] &= \sum_i \Lambda_i \\ b_0 \sum_i \omega_i + b_1 \sum_i \omega_i^2 + \dots + b_k \sum_i \omega_i^{k+1} + \sum_i \omega_i \arg[\text{FP}(\omega_i)] &= \sum_i \omega_i \Lambda_i \\ b_0 \sum_i \omega_i^k + b_1 \sum_i \omega_i^{k+1} + \dots + b_k \sum_i \omega_i^{2k} + \sum_i \omega_i^k \arg[\text{FP}(\omega_i)] &= \sum_i \omega_i^k \Lambda_i. \end{aligned} \tag{17}$$

The Fabry-Pérot effect term is replaced by its simple form according to Eq. (8), or

$$\begin{aligned}
 \sum_i \omega_i^k \arg [\text{FP}(\omega_i)] &= \sum_i \omega_i^k \{ \arg[1] - \arg [1 - \alpha_i \exp(-i\theta_i)] \} \\
 &= - \sum_i \omega_i^k \arg [1 - \alpha_i \cos \theta_i + i\alpha_i \sin \theta_i] \\
 &= - \sum_i \omega_i^k \arctan \left[\frac{\alpha_i \sin \theta_i}{1 - \alpha_i \cos \theta_i} \right] \\
 &\approx \sum_i \omega_i^k \left[\frac{\alpha_i \sin \theta_i}{\alpha_i \cos \theta_i - 1} \right]. \tag{18}
 \end{aligned}$$

The summation of the Fabry-Pérot term is negligible compared with $\sum_i \omega_i^k$ due to a rapid drop of α_i and a summation of the oscillating function. Therefore, fitting the argument of the transfer function, $\arg[H_{\text{meas}}(\omega)]$, by

$$f_2(\omega) = b_0 + b_1\omega + \dots + b_k\omega^k \tag{19}$$

could be used to remove the Fabry-Pérot term from the argument.

3.4. Estimating signal from simplified transfer function

As a result, the transfer function with no Fabry-Pérot effect is estimated from $f_1(\omega)$ and $f_2(\omega)$ which represents the amplitude and phase data respectively, or

$$\hat{H}(\omega) \equiv \exp [f_1(\omega) + if_2(\omega)] , \tag{20}$$

and the reflections are given by

$$E_{\text{FP}}(t) = \frac{1}{2\pi} \int_{-\infty}^{\infty} E_{\text{ref}}(\omega) [H(\omega) - \hat{H}(\omega)] \exp(i\omega t) d\omega . \tag{21}$$

However, since the polynomial fitting is carried out only over a part of the frequency range having high SNR, the primary signal directly determined from $\hat{H}(\omega)$ might lose accuracy. To preserve the form and total power of the probing signal, the primary pulse, $E(t)$, is then determined from

$$E(t) = E_{\text{sample}}(t) - E_{\text{FP}}(t) . \tag{22}$$

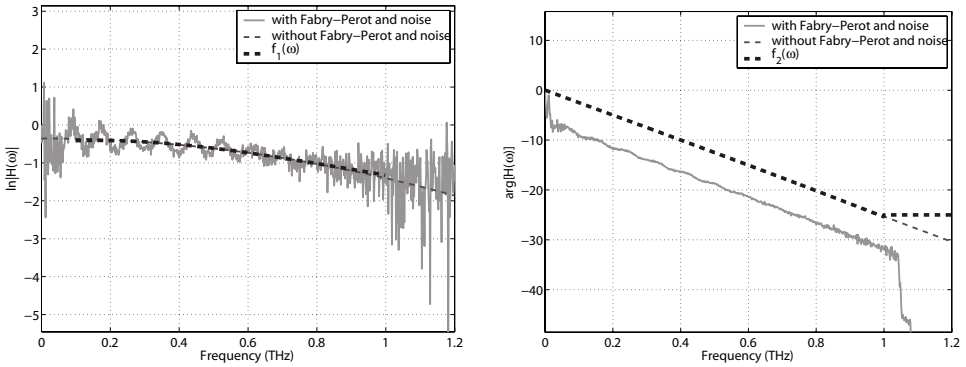
A limitation of the method is due to a restricted available terahertz signal bandwidth compared with an oscillation cycle of the Fabry-Pérot effect, or the sinusoidal terms in Eq. (11) and (18). If the bandwidth span is too short with respect to the oscillation cycle, the summations of the Fabry-Pérot term in Eqs. (11) and (18) might not yield small values. As a result, the Fabry-Pérot effect remains present. According to Eq. (9), a sample having large thickness, L , and large refractive index, n_{sample} , is required in order to produce short oscillation cycles of the Fabry-Pérot effect, whilst our signal has a limited bandwidth. Though, using a broadband terahertz system [14] overcomes the limitation of our method.

4. Simulation

A simulation is set up to illustrate the Fabry-Pérot removal performance under different conditions. The complex refractive index of a simulated material, modified from that of plain high-resistivity silicon, is $n_{\text{sample}} - i\kappa_{\text{sample}} = 3.42 - 0.1 \frac{\omega}{2\pi} i$, whereas the sample thicknesses are $500 \mu\text{m}$ for an optically thick sample and $50 \mu\text{m}$ for an optically thin sample. White Gaussian noise is added to the reference and probing terahertz signals so that they have an SNR of the order of 10 dB. Then, the transfer functions determined from noisy signals are fitted by polynomial order 3. To avoid the effect of noise in low power region of the spectra, we fit the polynomial to the transfer functions only from 0.1 to 1.0 THz.

4.1. Optically thick sample

Figure 1 shows the transfer function for the optically thick sample fitted by a third order polynomial. The fitted polynomial curve closely matches the curve of the transfer function without the presence of the Fabry-Pérot effect and noise. Note that



(a) Logarithm of the transfer function.

(b) Argument of the transfer function.

Fig 1. Transfer function for the optically thick sample fitted by polynomial order 3. The parameters for the transfer function are $L = 500 \mu\text{m}$ and $n_{\text{sample}} - \kappa_{\text{sample}} = 3.42 - 0.1 \frac{\omega}{2\pi} i$.

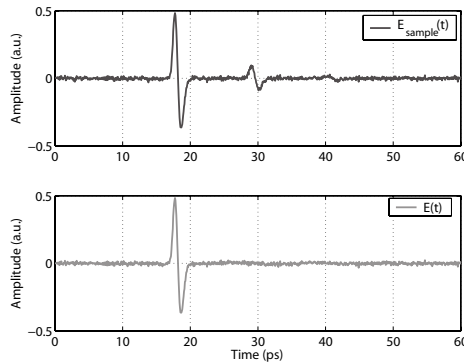


Fig 2. Probing terahertz signals for optically thick sample before and after the Fabry-Pérot removal is carried out, denoted by $E_{\text{sample}}(t)$ and $E(t)$, respectively.

the linearized phase unwrapping [5] is used for $f_2(\omega)$ to avoid false unwrapping in lower frequencies, resulting from noise. The signal after performing the Fabry-Pérot removal, compared with the original probing signal, is shown in Fig. 2. Clearly, two observable reflections following the primary pulse are removed from the signal with no effect on the existing noise. However, a small fluctuation occurs caused by the lack of higher and lower frequency information.

4.2. Optically thin sample

For the optically thin sample, our method performs poorly since the span of available frequencies, i.e., frequencies with high SNR, is too short compared with the oscillation of the sinusoidal function, according to Eq. (11) and (18). As shown in Fig. 3, the short span causes the polynomial to stickily track the oscillation rather than to average it out. When these polynomials are used to estimate the signal, they give the signal almost identical to the original one as shown in Fig. 4.

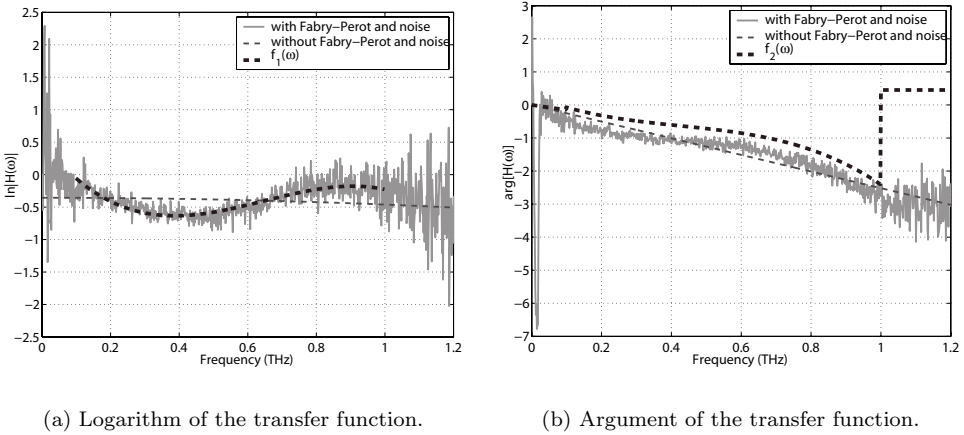


Fig 3. Transfer function for the optically thin sample fitted by polynomial order 3. The parameters for the transfer function are $L = 500 \mu\text{m}$ and $n_{\text{sample}} - \kappa_{\text{sample}} = 3.42 - 0.1 \frac{\omega}{2\pi} i$.

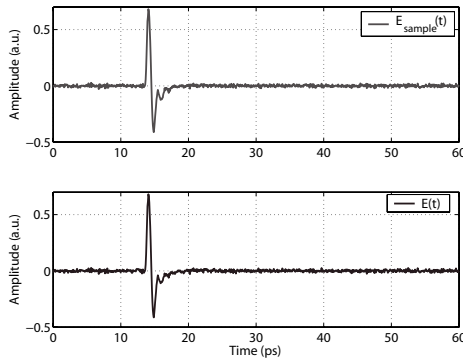


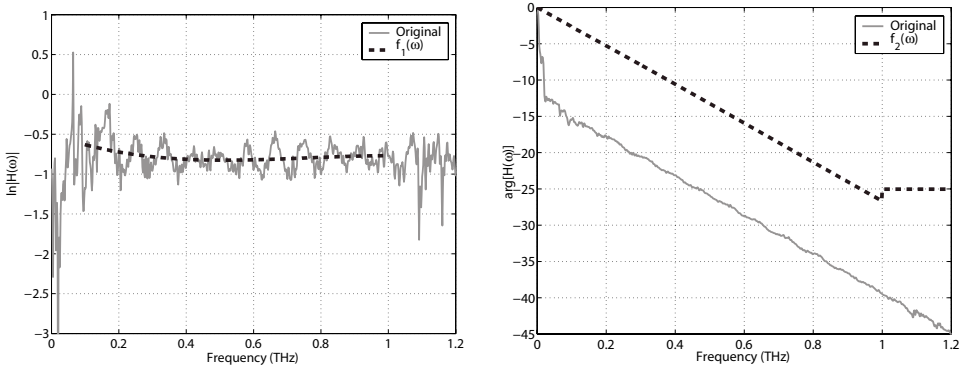
Fig 4. Probing terahertz signals for optically thin sample before and after the Fabry-Pérot removal is carried out, denoted by $E_{\text{sample}}(t)$ and $E(t)$, respectively.

5. Experimental Implementation

The implementation is carried out on a real T-ray signal probing a 525 μm -thick high-resistivity silicon wafer having the following characteristics: (i) polished on both sides, (ii) undoped, (iii) unbiased, (iv) $\langle 100 \rangle$ crystal orientation, and (v) bulk silicon. Two succeeding processes are demonstrated in this section. First, the proposed Fabry-Pérot removal is applied to the probing signal, giving a Fabry-Pérot free signal. In order to substantiate the result we subsequently perform a parameter estimation method on the Fabry-Pérot removed signal, and cross-validate obtained parameter values with those appearing in other literatures.

5.1. Removing Fabry-Pérot from the signal

Figure 5 shows the logarithm and argument of the transfer function for the high-resistivity silicon wafer fitted by $f_1(\omega)$ and $f_2(\omega)$, respectively. Similar to the simulation, the frequency range of the transfer function fitted by the polynomial is selected to be from 0.1 to 1.0 THz to reduce the effect of noise, and the polynomial order is 3. Note that the linearized phase unwrapping is employed again for $f_2(\omega)$.



(a) Logarithm of the transfer function.

(b) Argument of the transfer function.

Fig 5. Transfer function for the silicon wafer fitted by polynomial order 3.

The signal $E(t)$, estimated from $f_1(\omega)$ and $f_2(\omega)$, is shown in Fig. 6. The method significantly reduces the amplitude of the pulse located around 176 ps on the probing signal $E_{\text{sample}}(t)$. But a proof of that pulse being a reflection is required since fluctuation in $E(t)$ extends beyond this time, resulting in uncertainty in location of the reflection. If a sample with thickness L has a refractive index n_{sample} , we can estimate a location of the first reflection from

$$\Delta t = \frac{2n_{\text{sample}}L}{c}, \quad (23)$$

where Δt is the time period between the primary pulse and the first reflection. Succeeding reflections are also equally separated apart from one another by this time interval. Substituting the parameters of our sample¹ into Eq. (23), we expect

¹Refractive index n_{sample} of a high-resistivity silicon in terahertz region equals 3.418 [4]

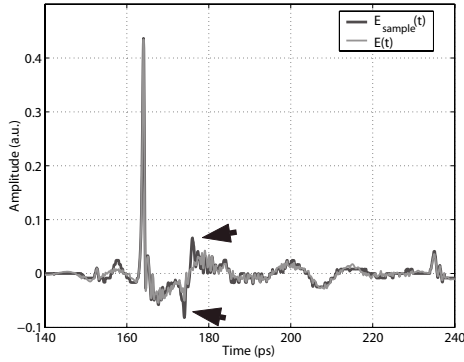


Fig 6. Probing terahertz signals for the silicon wafer before and after the Fabry-Pérot removal is carried out. The arrows indicate reduced amplitude of the pulse.

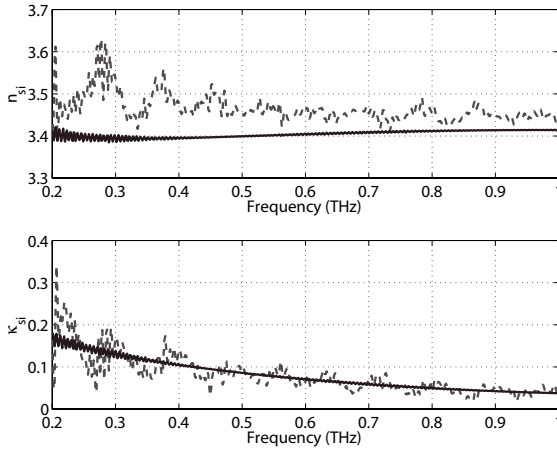


Fig 7. Refractive indices of the silicon wafer estimated from the unmodified signal (dash) and Fabry-Pérot removed signal (solid).

the first reflection lags the primary pulse by 11.97 ps. Obviously, our result shows two major pulses separated by 12 ps, confirming that the diminished pulse is the first reflection. Unfortunately, an observation for other reflections is not possible due to their magnitude being lower than the noise level.

5.2. Estimating material parameters from the processed signal

For comparison, the unmodified signal, $E_{\text{sample}}(t)$, and the Fabry-Pérot removed signal, $E(t)$, along with their reference $E_{\text{ref}}(t)$, are inputs to the gradient-based parameter estimation method (see Appendix A). The method yields two parameters of the silicon, n_{si} and κ_{si} , as shown in Fig. 7. Apparently, the parameters estimated from the Fabry-Pérot removed signal exhibit much lower variation than those estimated from the original signal. Cross validations with refractive indices of high-resistivity silicon, inspected by millimeter-wave in the 0.2 to 0.4 THz range [15], and by T-rays in the 0.2 to 1.0 THz range [4], show the concurrence.

6. Conclusions

The direct Fabry-Pérot removal is presented in this paper. By fitting polynomials to the logarithm and the argument of the transfer function, the Fabry-Pérot term is nearly eliminated. The new transfer function determined from the polynomials is used to regenerate the probing signal, which contains no reflection. The method performs successfully on the test sample, even if the noise or the fluctuation of the primary pulse perturbs the temporal location and amplitude of the reflections. Moreover, we have shown that the Fabry-Pérot free signal is appropriate for further processing such as the parameter extraction. The removal method requires no prior knowledge of material parameters, sample thickness, or pulse width. However, the method is limited to optically thick samples when the terahertz system provides a limited signal bandwidth.

Appendix A. Gradient Descent Search for Parameter Estimation

In this section we present a simple parameter estimation method, which is based on the method of gradient descent. The method estimates the refractive indices, n_{sample} and κ_{sample} , from the measured transfer function of the sample, which is obtainable from deconvolving the probing signal with respect to the reference.

For the sake of completeness the equations for logarithm and argument of transfer function are restated here as follows:

$$\ln |H(\omega)| = \ln \left| \frac{4\tilde{n}_{\text{sample}}\tilde{n}_{\text{air}}}{(\tilde{n}_{\text{sample}} + \tilde{n}_{\text{air}})^2} \right| - \kappa_{\text{sample}} \frac{\omega L}{c} + \ln |\text{FP}(\omega)|, \quad (\text{A.1})$$

and

$$\arg[H(\omega)] = \arg \left[\frac{4\tilde{n}_{\text{sample}}\tilde{n}_{\text{air}}}{(\tilde{n}_{\text{sample}} + \tilde{n}_{\text{air}})^2} \right] - (n_{\text{sample}} - n_{\text{air}}) \frac{\omega L}{c} + \arg[\text{FP}(\omega)]. \quad (\text{A.2})$$

Note that using the above equations means the Fabry-Pérot effect is taken into account while the parameters are estimates. As in this paper we remove the effect from a signal prior to the estimation, the Fabry-Pérot terms in Eq. (A.1) and (A.2) must be dropped to avoid redundancy.

An error term, which is the difference between the model transfer function $H(\omega)$ and the measured transfer function $H_{\text{meas}}(\omega)$ at a specific angular frequency ω , is defined by [5]

$$\delta(n_{\text{sample}}, \kappa_{\text{sample}}) = \delta\rho^2 + \delta\varphi^2, \quad (\text{A.3})$$

where

$$\begin{aligned} \delta\rho &= \ln |H(\omega)| - \ln |H_{\text{meas}}(\omega)|, \\ \delta\varphi &= \arg(H(\omega)) - \arg(H_{\text{meas}}(\omega)). \end{aligned} \quad (\text{A.4})$$

Since $\arg(H(\omega))$ and $\ln |H(\omega)|$ are primarily influenced by $-(n_{\text{sample}} - n_{\text{air}}) \frac{\omega L}{c}$ and $-\kappa_{\text{sample}} \frac{\omega L}{c}$, respectively, a plot of error function against the complex refractive index appears paraboloid-like (see Fig. A.1).

The gradient descent method is introduced to find the nearest local minimum, at which n_{sample} and κ_{sample} are located. The intermediate refractive indices are

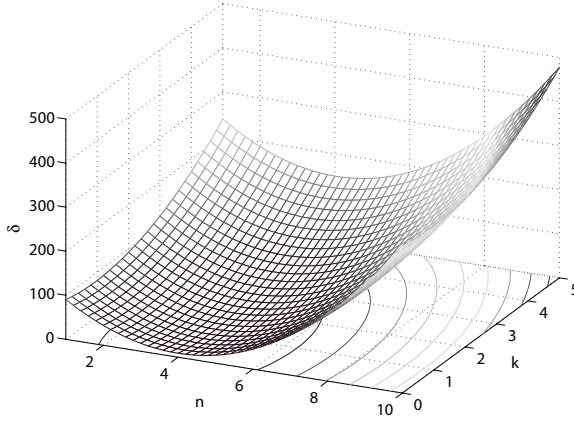


Fig A.1. Error function plotted against complex refractive index $n + i\kappa$, where $n_{\text{sample}} = 4$, $\kappa_{\text{sample}} = 1$, and $\omega L/c = 3$. The range of refractive indices covers all values found in normal materials. After Duvillaret, et al [5].

iteratively and alternately updated by local downhill gradients, or

$$\begin{aligned} n_i &= n_{i-1} - \epsilon \delta_n(n_{i-1}) , \\ \kappa_i &= \kappa_{i-1} - \epsilon \delta_\kappa(\kappa_{i-1}) . \end{aligned} \tag{A.5}$$

We approximate the partial derivatives of the error w.r.t. n and κ by

$$\begin{aligned} \delta_n &= -2 \frac{\omega L}{c} \{ \arg(H(\omega)) - \arg(H_{\text{meas}}(\omega)) \} , \\ \delta_\kappa &= -2 \frac{\omega L}{c} \{ \ln |H(\omega)| - \ln |H_{\text{meas}}(\omega)| \} , \end{aligned} \tag{A.6}$$

respectively. Dorney *et al.* [7] proposed that the reasonable update step size, ϵ , is constant and equal to 0.01. However, in Eq. (A.6) the angular frequency, appearing explicitly and implicitly in $\arg(H(\omega))$ and $\ln |H(\omega)|$, cause the inconsistency of update step over the range of frequency. For example, the convergence of complex refractive index at lower frequency is slower than that at higher frequency, and sometimes divergence occurs at higher frequency as the update step is too large. Hence, to solve this problem we remove $\omega L/c$ terms from the partial derivatives,

$$\begin{aligned} \delta_n &= - \{ \arg(H(\omega)) - \arg(H_{\text{meas}}(\omega)) \} , \\ \delta_\kappa &= - \{ \ln |H(\omega)| - \ln |H_{\text{meas}}(\omega)| \} , \end{aligned} \tag{A.7}$$

and use an adaptive step size,

$$\epsilon = \hat{\epsilon} \frac{c}{\omega L} , \tag{A.8}$$

where a proper $\hat{\epsilon}$ is in between 0.01 and 0.1.

References

- [1] Q. Wu and X.-C. Zhang, Free-space electro-optic sampling of terahertz beams, *Applied Physics Letters* **67**(24) (1995) 3523–3525.
- [2] D. M. Mittleman, R. H. Jacobsen and M. C. Nuss, T-ray imaging, *IEEE Journal of Selected Topics in Quantum Electronics* **2**(3) (1996) 679–692.
- [3] D. M. Mittleman, M. Gupta, R. Neelamani, R. G. Baraniuk, J. V. Rudd and M. Koch, Recent advances in terahertz imaging, *Applied Physics B: Lasers and Optics* **68**(6) (1999) 1085–1094.
- [4] D. Grischkowsky, S. Keiding, M. van Exter and Ch. Fattinger, Far-infrared time-domain spectroscopy with terahertz beams of dielectrics and semiconductors, *Journal of the Optical Society of America B* **7**(10) (1990) 2006–2015.
- [5] L. Duvillaret, F. Garet and J.-L. Coutaz, A reliable method for extraction of material parameters in terahertz time-domain spectroscopy, *IEEE Journal of Selected Topics in Quantum Electronics* **2**(3) (1996) 739–746.
- [6] L. Duvillaret, F. Garet and J.-L. Coutaz, Highly precise determination of optical constants and sample thickness in terahertz time-domain spectroscopy, *Applied Optics* **38**(2) (1999) 409–415.
- [7] T. D. Dorney, R. G. Baraniuk and D. M. Mittleman. Material parameter estimation with terahertz time-domain spectroscopy. *Journal of the Optical Society of America A* **18**(7) (2001) 1562–1571.
- [8] W. Withayachumnankul, B. Ferguson, T. Rainsford, S. P. Mickan and D. Abbott, Material parameter extraction for terahertz time-domain spectroscopy using fixed-point iteration in *Proc. SPIE Photonic Materials, Devices, and Applications*, (ed.) G. Badenes, Vol. 5840 (2005), pp. 221–231.
- [9] W. Withayachumnankul, B. Ferguson, T. Rainsford, S. P. Mickan and D. Abbott, Simple material parameter estimation via terahertz time-domain spectroscopy, *IEEE Electronics Letters* (2005), in press.
- [10] C. C. Te, B. Ferguson and D. Abbott, Investigation of biomaterial classification using T-rays in *Proc. SPIE Biomedical Applications of Micro- and Nanoengineering*, (eds.) Dan V. Nicolau and Abraham P. Lee, Vol. 4937 (2002), pp. 294–306.
- [11] R. H. Jacobsen, D. M. Mittleman and M. C. Nuss. Chemical recognition of gases and gas mixtures with terahertz waves, *Optics Letters* **21**(24) (1996) 2011–2013.
- [12] B. Ferguson, S. Wang, D. Gray, D. Abbott and X.-C. Zhang, Identification of biological tissue using chirped probe THz imaging, *Microelectronics Journal* **33**(12) (2002) 1043–1051.
- [13] B. Ferguson, S. Wang, D. Abbott and X.-C. Zhang. Powder detection with THz imaging in *Proc. SPIE Terahertz for Military and Security Applications*, (eds.) R. J. Hwu and D. L. Woolard, Vol. 5070 (2003), pp. 7–16.
- [14] P. Y. Han and X.-C. Zhang, Free-space coherent broadband terahertz time-domain spectroscopy, *Measurement Science and Technology* **12**(11) (2001) 1747–1756.
- [15] M. N. Afsar and K. J. Button, Precise millimeter-wave measurements of complex refractive index, complex dielectric permittivity and loss tangent of GaAs, Si, SiO₂, Al₂O₃, BeO, macor, and glass, *IEEE Transactions on Microwave Theory and Techniques* **MTT-31**(2) (1983) 217–223.

Copyright of *Fluctuation & Noise Letters* is the property of World Scientific Publishing Company and its content may not be copied or emailed to multiple sites or posted to a listserv without the copyright holder's express written permission. However, users may print, download, or email articles for individual use.